Innovative Synthesis of Fe Doped ZnO-Zeolite Composite for Advanced Applications

Akmal Shahzad Babar, Shahzad Ali Shahid Chatha* and Atta Ul Haq
Department of Chemistry, Government College University Faisalabad 38000, Pakistan.
saschatha@gcuf.edu.pk*

(Received on 1st January 2025, accepted in revised form 16th July 2025)

Summary: This study introduces an innovative approach for synthesizing an Fe-doped ZnO-zeolite composite material with enhanced structural and functional properties targeting advanced environmental and catalytic applications. The key hypothesis of this study is that Fe doping and zeolite integration can synergistically increase the performance of ZnO by increasing the surface area, structural stability and reactivity. Fly ash-based zeolites were synthesized by fusion-assisted hydrothermal technique and employed as a support matrix for ZnO nanoparticles. ZnO was doped with varying concentrations of Fe (0.5–2 wt.%) to analyze the impact of iron incorporation on crystallinity and morphology. Subsequently, Fe-ZnO was composited with zeolite to make a hybrid material with multifunctional characteristics. Comprehensive characterizations were performed via SEM (to observe morphology and dispersion), FTIR (to confirm bonding and functional groups) and XRD (to analyze crystal structure and phase purity). XRD results confirmed the presence of wurtzite ZnO structure with no secondary phases, while SEM micrographs revealed even dispersion of Fe-ZnO on zeolite surfaces. Notably, Fe doping caused a slight shift in the diffraction peaks and reduced the crystallite size (~18–25 nm), confirming the successful incorporation of Fe into the ZnO lattice. FTIR spectra validated the coexistence of Zn–O, Fe–O, and zeolitic Si–O–Al bonds. The efficient integration of Fe-ZnO nanoparticles into the zeolite framework is confirmed by the different peaks in the Raman spectra at around 300, 445, 620, and 1050 cm^{-1}. The BET studies revealed that the Fe-ZnO/Zeolite composite has an average pore diameter of 4.7 nm and a balanced micro-mesoporous structure with an intermediate surface area. These results support the hypothesis and indicate that the Fe-ZnO/zeolite composite possesses tailored chemical and morphological properties, making it suitable for applications in adsorption, catalysis, and environmental remediation. Future work can explore optimization strategies and performance metrics for specific pollutant degradation or catalytic conversions.

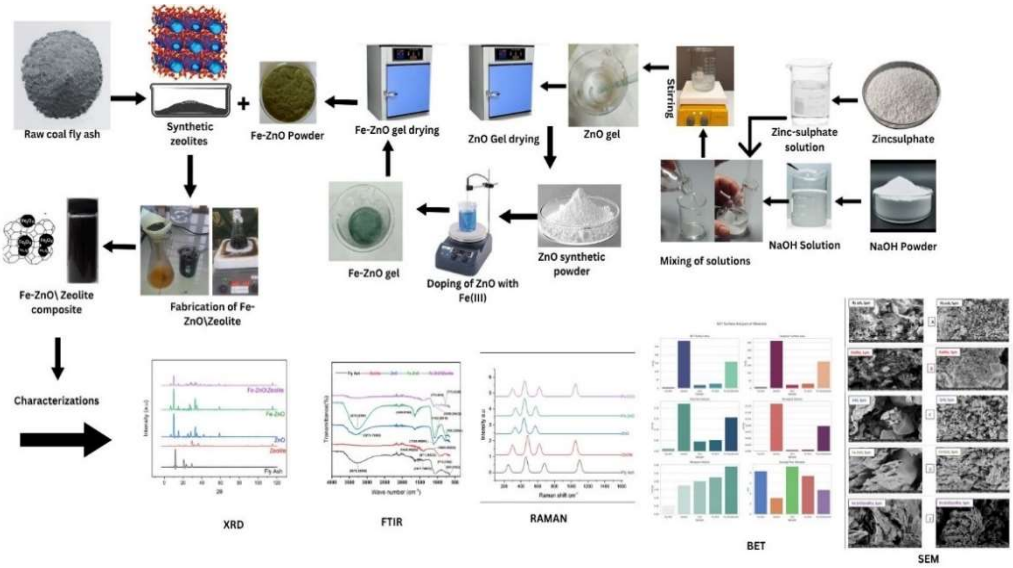

Keywords: Fly ash; Zeolites; Fe doped ZnO; Composite; Characterization; SEM Analysis.

Introduction

Zinc oxide (ZnO) is a widely synthesized, practiced and inexpensive material [1]. After iron, it is considered the second most common metal, which is safe and easy to work with. It is used in various materials, including paints, adhesives, ointments, sealants, plastics, pigments, ceramics, cement, glass,

*To whom all correspondence should be addressed.

lubricants, rubber, food, batteries, ferrites and fire retardants [2]. It is an n-type semiconductor with a wide band gap of energy 3.37 eV and a binding energy of 60 meV [3]. Wide band gap, high exciton binding energy and significant photocatalytic activity are some of the desired characteristics of zinc oxide (ZnO), a semiconductor that has been extensively explored. However, fast electron-hole recombination and low absorption of visible light frequently restrict ZnO's practical effectiveness. To overcome these limitations, doping ZnO-based systems with transition metals (such as Fe) has been investigated as a way to modify the band structure and increase the effectiveness of charge separation [4-5].

ZnO has been synthesized using various methods, including hydrothermal and combustion, as well as the sol–gel co-precipitation method [6]. The sol–gel method is reported to be more economical and environmentally friendly [7]. It has been discovered that the most efficient method for inducing structural advancements in ZnO is metal ion doping. Doping can induce ferromagnetism in semiconductors with a very minute quantity of transition metal [8]. Iron (Fe-III) is considered one of the best dopants for ZnO due to its comparable ionic radius and well-reported chemical stability. The incorporation of Fe into the ZnO structure is relatively safe for maintaining the structural properties of the crystal [9]. ZnO-based materials face a drawback of reduced quantum efficiency when applied as photocatalysts due to the recombination of electron-hole pairs, which can waste energy as heat or light [10-11]. Many researchers have attempted to create composite materials by immobilizing nanoparticles on suitable porous and inert substances such as zeolites, silica, alumina and activated carbon [12-13]. Zeolites are considered more suitable among the multiple reported types of porous materials because of their unique characteristics, which include a large surface area, chemical properties, high heat stability and both hydrophobic and hydrophilic attributes, as well as an environmentally friendly nature [14].

Zeolites are crystalline, hydrated, microporous aluminosilicates characterized by a network of linked pores formed by a 3D structure of tetrahedral Al and Si [15]. Synthesizing zeolites from chemical sources such as silicates and pure aluminates is costly. Expenses can be reduced by utilizing natural sources or byproducts as raw materials. [16]. Researchers have been exploring natural resources, waste products, or industrial byproducts to produce economically viable zeolites. Fly ash, an industrial waste, has been used in several studies for the synthesis of zeolites. Fly ash is a well-documented material for zeolite synthesis because it has a composition similar to volcanic materials, characterized by high SiO_2 and Al_2O_3 content [17]. The hydrothermal method is often used to synthesize zeolites from fly ash. The alkaline fusion preceding the hydrothermal treatment involves fusing fly ash with a specific amount of NaOH at a suitable temperature to produce Na-zeolites [18].

Metal-doped ZnO and ZnO–zeolite composites have been synthesized individually in the past. However, comprehensive research into the synergistic coupling of Fe-doped ZnO with zeolite frameworks is still lacking. Most of the documented methods either produce poor dopant dispersion or lack control over particle shape, which ultimately reduces functional efficiency [19-20]. The fabrication of iron (Fe)-doped zinc oxide (ZnO)/zeolite composite materials is the primary focus of this study, aiming to enhance the properties of ZnO for various applications including photocatalysis, wastewater treatment and energy storage. Additionally, integrating ZnO with porous zeolite matrices is an effective way to improve dispersion, prevent nanoparticle agglomeration, and increase surface basicity, all of which can further enhance photocatalytic and adsorptive activities [21].

Advanced characterization techniques, including scanning electron microscopy (SEM), Fourier-transform infrared spectroscopy (FTIR), and X-ray diffraction (XRD), were adopted to investigate the synthetic products. It also makes a significant contribution to the growing field of materials and composites. The successful synthesis and characterization of these novel materials can pave the way for future research on composite optimization, scalability and photocatalytic applications.

The current work focuses on the novel synthesis of Fe-doped ZnO–zeolite composites using a controlled sol-gel technique to address the aforementioned gaps. In addition to provide scalability and environmental friendliness, this method ensures uniform doping and fine nanoparticle dispersion within the zeolite framework, making it appealing for practical applications. To demonstrate its potential for cutting-edge environmental and energy-related applications, the work aims to provide a thorough structural, morphological and functional characterization, with a focus on photocatalytic and adsorption performance.

Experimental

Chemicals and reagents

All the chemicals and reagents used in this study were of analytical grade; zinc sulfate heptahydrate ($ZnSO_4 \cdot 7H_2O$) from Merck, iron (II) sulfate

heptahydrate ($FeSO_4 \cdot 7H_2O$) from Sigma-Aldrich, sodium hydroxide (NaOH, ≥98%) from Loba Chemie, and ethanol (C_2H_5OH, ≥99.5%) from Merck. Deionized water, produced by an in-laboratory distillation system at the Department of Chemistry, Government College University, Faisalabad, was used throughout all experimental stages.

Synthesis of fly ash-based zeolites

Raw fly ash (rFA) samples were collected by a random stratified sampling method from coal-fired power plants located in the Faisalabad region of Pakistan. The collected samples were sieved through an 80-micron mesh to eliminate coarse particles larger than 150–200 µm, ensuring a fine and uniform particle size distribution. Zeolites were synthesized via a fusion-assisted hydrothermal technique by following the literature-reported methodology with slight modifications [22]. The sieved fly ash was fused with sodium hydroxide (NaOH) in a 1:1 weight ratio at 550 °C for 1.5 hours in a muffle furnace (B-170, Nabertherm). Then 20 grams of the fused product were dissolved in double-distilled water (DD-H_2O) at a 1:2 weight ratio to form an amorphous gel. The resulting gel was thoroughly washed and adjusted to a pH of 8. It was then dried at 80°C in a microwave heating oven (ENR-38XDG, JW-Enviro) for 12 hours and stored in polythene air-tight bags for further experimentation.

Synthesis of Fe-doped ZnO nanoparticles

Fe-doped ZnO nanoparticles were synthesized through a two-step process. Initially, 100 mL of a 0.5 M zinc sulfate heptahydrate ($ZnSO_4 \cdot 7H_2O$) solution and 25 mL of a 0.5 M sodium hydroxide (NaOH) solution were prepared separately. NaOH solution was added dropwise to the zinc sulfate solution while stirring continuously at 600 rpm until white, gel-like foam formed. The precipitates were then filtered, washed with distilled water and dried for 8 hours at 100°C. After drying, the powder was ground and calcined at 500°C [23]. Following detailed characterization and analysis, Fe doping of ZnO powder was performed in the second step using a reported co-precipitation method [24]. The synthesized Fe-ZnO composite was thoroughly characterized and analyzed, then stored in airtight polypropylene tubes for further experiments.

Synthesis of Fe-ZnO/Zeolite composite material

The synthesized zeolites and Fe-ZnO materials were ground to ensure homogeneous products. An appropriate amount of Fe-doped ZnO powder was then calculated based on the zeolite amount to ensure that 30% of its weight was dissolved in ethanol. The controlling agent ensures consistency and prevents agglomeration. After grinding for 30 minutes, the mixture was spread on a glass plate and dried in an oven (TK/L G 154, Ehret) at 60°C to eliminate ethanol and moisture. Subsequently, the synthesized composite material was characterized thoroughly [25].

Characterization

The advanced techniques were employed in this study for the characterization of the synthesized material. The mineralogical compositions and crystallinity of fly ash, zeolite, ZnO, Fe-ZnO, and Fe-doped zeolite composite were analyzed using powdered XRD analysis (MiniFlex600-C, Japan) with Cu-Kα radiation. The morphology of the research products was analyzed using a Scanning Electron Microscope (Apreo S, Thermofisher Scientific, Eindhoven, Netherlands) set to HV = 5 kV, Signal A = SE1, and a working distance of 6.1 mm. The specific surface area of the porous materials was measured using BET surface area analysis. The functionality and surface chemistry of the synthesized products were examined through FTIR spectroscopy (Cary 630, Agilent Technologies FTIR) within a scanning range of 4000-500 cm^{-1}. For Fe-doped ZnO materials, the Scherrer method is a primary technique used to estimate crystallite size. This method relies on X-ray diffraction (XRD) peak broadening and is described by the following formula:

$$D = K\lambda/\beta\cos\theta \quad (1)$$

Here λ is the X-ray wavelength, D is the average crystallite size, K is a shape factor (calculated as 0.9), β is the full width at half maximum (FWHM) of the diffraction peak, and θ is the Bragg angle [26]. This method yields crystallite sizes that generally range from 6 to 97 nm across various investigations [27].

In contrast to the Scherrer technique, the Williamson-Hall (W-H) method offers a more advanced approach for analyzing crystallite size, taking into consideration both strain-induced and size-induced broadening in X-ray diffraction patterns. It is presumed that crystallite size effects exclusively cause peak broadening; the W-H analysis distinguishes between these two contributions using equation 2 [28].

$$\beta\cos\theta = K\lambda/D + 4\varepsilon\sin\theta \quad (2)$$

Where K is the form factor, λ is the X-ray wavelength, D is the crystallite size, ε is the macrostrain, β is the FWHM, and θ is the Bragg angle [28]. Both the Scherrer and Williamson-Hall approaches have been used in this study to investigate the crystallite properties of the synthesized composite material.

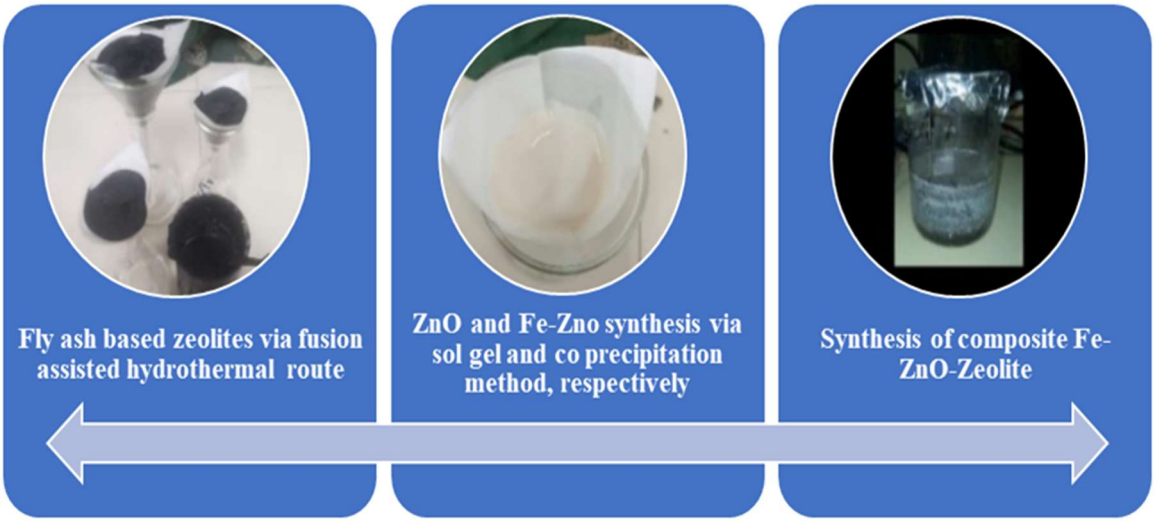

Fig. 1: Systematic synthesis of Fe-ZnO-zeolite composites.

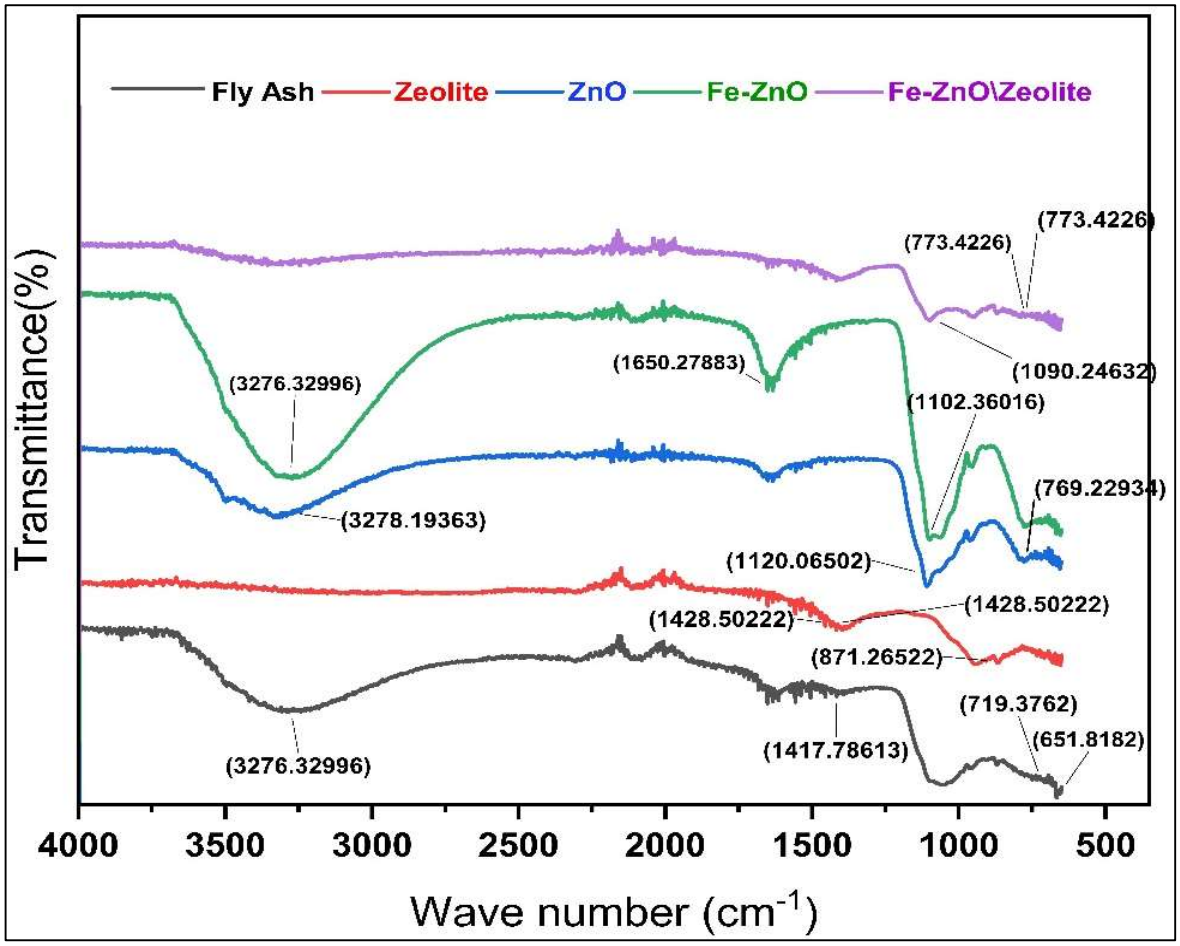

Fig. 2: FTIR specta of Fly ash, Zeolite, ZnO, Fe-ZnO and Fe-ZnO-zeolite composite.

Results and Discussion

FTIR study of synthesized materials

FTIR spectra of fly ash (FA) and synthetic zeolite revealed notable variations, which are shown in Fig 2. The zeolite materials exhibited a band in the 600 cm-1 range, identified as the Si/Al–O bending vibrations. The symmetrical stretching in the direction of Al–O–Al and Si–O–Si indicates double ring vibrations at about 600–670 cm^{-1} [29-30]. The fusion process exhibits Si-O-Si and Al-O-Al stretching vibrations in the range of 720–610 cm^{-1}. These vibration bands are ascribed to the zeolites and can be linked to the alkaline activation [30]. Bending vibrations appearing in raw fly ash in the range of 1100 to 1200 cm^{-1} and 800 to 900 cm^{-1} represent mullite and quartz, and a prominent vibration band appeared at 871 cm^{-1} in synthetic zeolite, verifying a gradual transformation of fly ash minerals into zeolites. The existence of aluminates and silicates in the synthetic zeolite materials is indicated by a prominent dip that appears in FA at 1417 cm^{-1} and in zeolite at 1428 cm^{-1}. The vibrations at 3200 to 3400 cm^{-1} and 1600 to 1650 cm^{-1} indicate water molecules. The presence of water is shown at 3276 cm^{-1} in the fly ash sample, and its disappearance in zeolites suggests the absence of water content [31]. In the FTIR study of synthesized ZnO, the region between 600 and 800 cm^{-1} provides information corresponding to symmetric Zn-O-Zn vibrations. The IR dip near 769 cm^{-1} represents unsymmetrical stretching vibrations of Zn-O-Zn bonds. Additionally, the dip at 1120 cm–1 indicates the presence of Zn-OH bending vibrations [32]. The current study suggests that Zn–O bonding often exhibits absorption bands in the fingerprint region below 1000 cm-1, as shown in Fig 2. FTIR study investigation of Fe-ZnO material has identical spectra to the literature with the existence of many distinct bands at 1102, 1650, and 3276 cm^{-1} [33-35]. The FTIR studies of the Fe-ZnO zeolite composite reveal significant dips in the Si-O-Si stretching vibrations, which are asymmetric and appear at 1090 cm^{-1} and some minor changes for that material appear in the 1082–1074 cm^{-1} range. Fe-O and Zn-O stretching vibrations give rise to absorption bands within the range of 600–700 cm^{-1}, indicating the presence of metal oxides in the synthesized composite [36]. The vibrations of Al-O-Si and Si-O-Si bonds in the zeolite framework are represented as bands between 900 and 1100 cm^{-1}, showing the zeolite's structural integrity is a composite material [37]. Our findings demonstrated that Al and Si make up the main composition of fly ash, which can serve as precursors of aluminosilicate for the synthesis of zeolites [38]. These properties demonstrated the practical synthesis of Fe-ZnO/zeolite composites, where both the metal oxides and zeolite properties persist into the material.

SEM analysis

Fig. 3 shows the morphology of the synthesized products and raw materials. It illustrates the uneven shape of fly ash in contrast to the synthetic zeolite samples. The FA composition contains the quartz (A) and mullite (Q) phases, but also displays amorphous silica and alumina remnants that describe the morphological conformations, as shown in micrographs [39]. After being treated and purified, fly ash adopts a characteristic shape [40]. SEM images of zeolite at magnifications of 1 and 5µm in Fig. 3A represent its crystal structure. Apart from the visible crystals, a relatively homogeneous matrix is observed, which is attributable to a combination of microcrystalline phases and an amorphous bulk [41]. Fig. 3B shows the SEM images of ZnO nanoparticles at a magnification that confirms the nanosize range of the synthesized particles, aligning with the published data [42]. SEM pictures of Fe-doped ZnO reveal the aggregation of ZnO, resulting in a decrease in particle size and a rise in characteristic surface area [43]. It demonstrates identically sized, spherical ZnO nanoparticles on the zeolite surface of the evaluated material, aligning with previous studies [44]. Fig. 3E demonstrates that the Fe-ZnO/Zeolite exhibits a structure with rhombic dodecahedrons, having diameter of around 80 nm [45]. The chain structure of ZnO is not visible in the composite; instead, the ZnO is integrated as agglomerates that are dispersed evenly over the zeolitic surface during the stirring process.

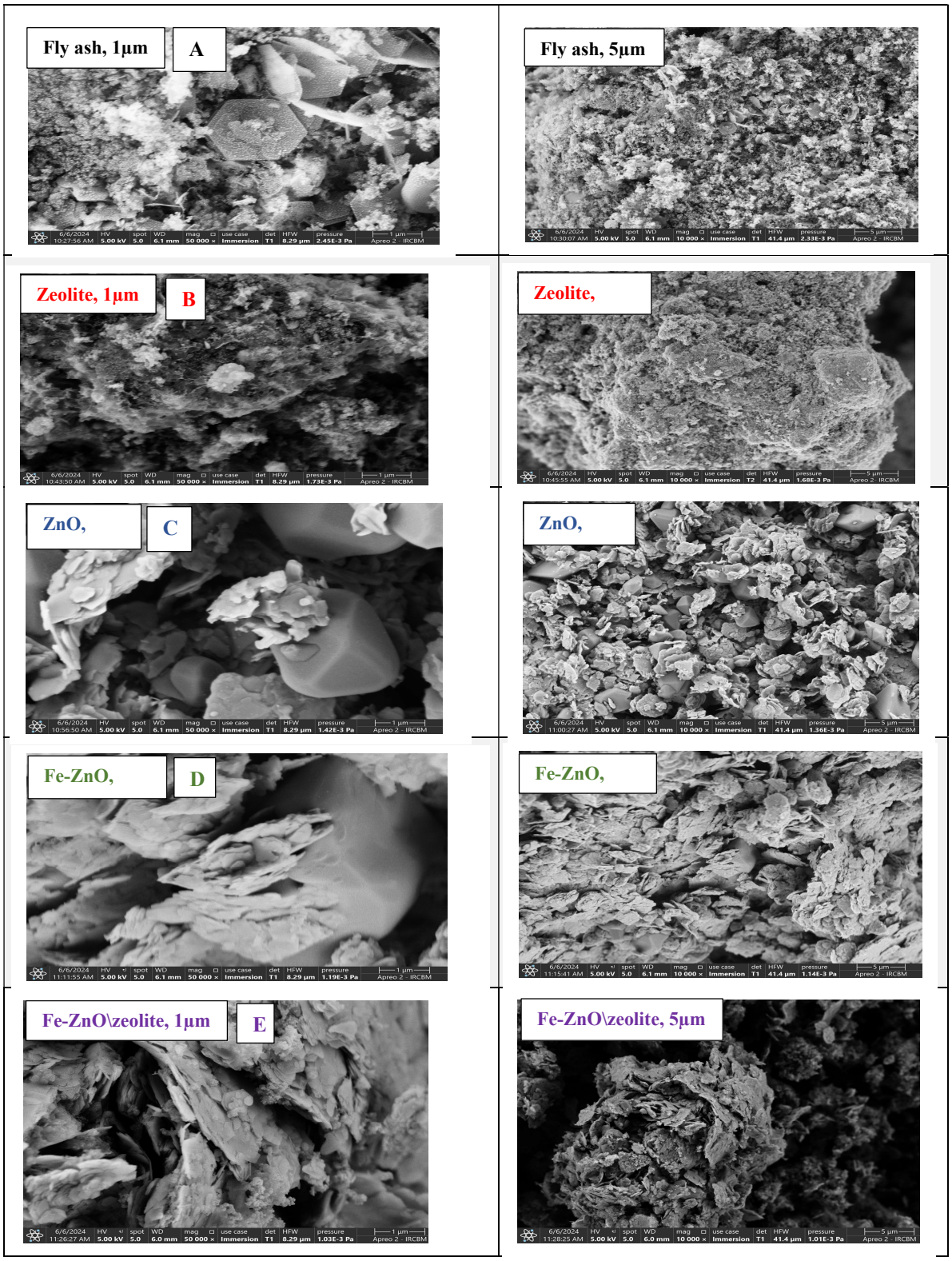

Fig. 3: SEM images of raw and synthesized products at 1 and 5µm.

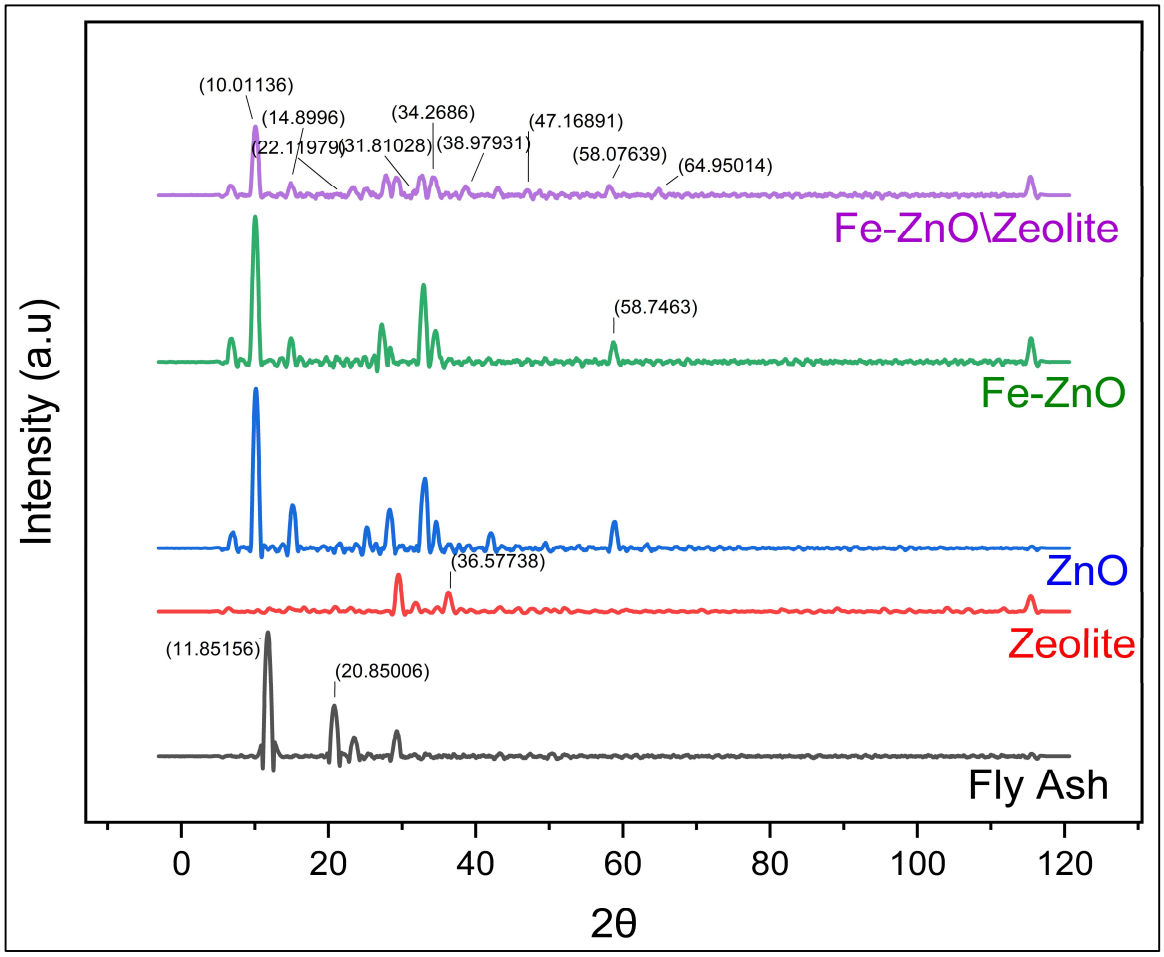

Fig. 4: XRD analysis of raw and synthesized materials.

XRD studies

Fly ash is primarily composed of minerals with varying ratios of silica and alumina, as observed in the XRD patterns (Fig. 4). The synthesized products exhibit peaks corresponding to the crystalline phases of hydroxyl sodalite and alumina, as reported in the literature [39]. Previous studies have observed that the mineral phases formerly present in fly ash were absent in the synthesized zeolite [46]. The quartz peaks in zeolites are more pronounced compared to those in fly ash, suggesting that the material rearranges in an alkaline medium [47]. The production of Na-zeolites is noticed after an in-depth analysis. As shown in Fig. 4, ZnO exhibits prominent diffraction peaks at approximately 31.8°, 34.4°, 36.3°, 47.5° and 56.6°, indicating a distinctive wurtzite structure [48]. The XRD patterns of Fe^{+3}-doped ZnO are also shown in Fig. 4. The diffracted peaks shifted to larger angles due to tensile stress induced by lattice deformation, also reported in the literature [24]. The presence of additional sharp peaks at approximately 60° confirms the presence of Fe atoms in the crystal structure, as also elaborated in the published data [49]. The ZnO structure is represented by the diffraction peaks at 2θ = 58.07° and 63.95°. In contrast, the doping material's structural characteristics are responsible for the diffraction peaks at 2θ = 31.81°, 34.26°, 38.97° and 47.16° in the Fe-ZnO/zeolite and are comparable with the published data [50]. This is consistent with the literature, as XAFS investigations indicated Fe^{3+}/Fe^{2+} substitution into Zn sites, resulting in a shift in peak locations and a decrease in crystallite size [51]. The composite Fe-ZnO/Zeolite exhibits a range of peaks from both the ZnO and zeolite phases, suggesting good integration. The obtained results exhibited unique properties in ZnO/zeolite composites, emphasizing improved dispersion and synergistic benefits in

photocatalytic and adsorption applications. The fly ash-derived zeolite acts as a support, preventing the agglomeration of ZnO nanoparticles and increasing their surface area and reactivity [52]. XRD analysis of the composite material revealed the presence of additional peaks at angles of 2θ = 10.01°, 14.89°, and 22.11°, indicating the persistence of synthetic zeolites in the final product [51].

Scherrer and Williamson-Hall approaches

The crystallite size of the synthesized composite was calculated using the Scherrer equation based on the full width at half maximum (FWHM) of notable XRD peaks, as mentioned in Fig. 4. Calculations in this work were based on the primary diffraction peak at around 2θ = 36.57°, which corresponds to the ZnO (101) plane. The average crystallite size of ZnO was determined to be around 32 nm. The lattice strain suggests that controlled crystal formation is the reason for the crystallite size to drop to around 27 nm. The Fe–ZnO particles further reduced their crystallite size to approximately 22–25 nm when integrated into the zeolite matrix, indicating improved particle dispersion and controlled size. These findings are consistent with previous research on ZnO nanostructures doped with metals [53]. The line's slope obtains the strain, and the y-intercept gives the crystallite size. The ZnO sample showed no strain due to its great crystallinity. Nonetheless, Fe–ZnO showed a rise in lattice strain (about 0.004–0.006), indicating that the dopant addition created internal stress. The computed strain values in the Fe–ZnO/zeolite composite were greater (about 0.005–0.007), indicating that more substantial lattice distortions appeared due to the interaction of ZnO nanoparticles with the zeolite matrix. It is reported that these strain-induced distortions produce defect states and oxygen vacancies, which can enhance photocatalytic performance and surface activity [54]. In contrast to earlier research, the Fe–ZnO/zeolite composite produced in this study exhibited a smaller crystallite size and a greater microstrain, which are advantageous for several cutting-edge applications, including photocatalysis, hydrogen evolution, and adsorption procedures. In conclusion, the structural analysis using the Williamson-Hall and Scherrer methods confirmed that the Fe doping into ZnO was successful, and a well-integrated Fe–ZnO/zeolite composite was synthesized

Raman studies

The vibrational properties of fly ash, zeolite, ZnO, Fe-ZnO, and the synthesized Fe-ZnO/zeolite composite were analyzed by the Raman spectra as shown in Fig. 5. Distinctive bands at about 250–300 cm^{-1}, 460 cm^{-1}, 680 cm^{-1}, and 1100 cm^{-1} indicates the presence of Si–O–Si stretching and bending vibrations [55]. As compared to fly ash, the zeolite spectrum shows more distinct and sharper peaks, especially at 300 cm^{-1}, 480 cm^{-1}, 620 cm^{-1}, and 1050 cm^{-1}. The symmetric stretching of Si–O–Al and Si–O–Si bonds, which is characteristic of crystalline aluminosilicate frameworks, is responsible for these peaks. The synthesis of zeolitic frameworks is confirmed by the appearance of band at around 480 cm^{-1}, which is linked to internal T–O–T bending vibrations (T = Si or Al). A similar Raman activity in synthetic zeolites made from ash has been reported in the literature [56]. ZnO has discrete peaks at 437 cm^{-1}, which are characteristic of wurtzite ZnO. Additionally, the small peaks associated with vibrations due to oxygen vacancies are seen at 330 cm^{-1} and 570 cm^{-1}. The successful synthesis was confirmed by these characteristics, which closely resemble to Raman spectra of pure ZnO nanoparticles reported in literature [57]. The Fe-doped ZnO material's spectrum showed somewhat shifted and wider peaks, particularly at 445 cm^{-1} and 575 cm^{-1}. These changes represent the addition of Fe ions to the ZnO crystal matrix, as well as changes in lattice structure, following previous literature [58]. Fe-ZnO and zeolite characteristic peaks are combined to form the prominent changes in the composite spectra. It is confirmed that the Fe-ZnO nanoparticles have successfully integrated into the zeolite matrix by the appearance of peaks at about 300 cm^{-1}, 445 cm^{-1}, 620 cm^{-1}, and 1050 cm^{-1}. Vibrational characteristics indicated excellent dispersion and no structural deterioration, which is well aligned with the literature studies on ZnO/zeolite and Fe-doped ZnO/zeolite composite materials [58].

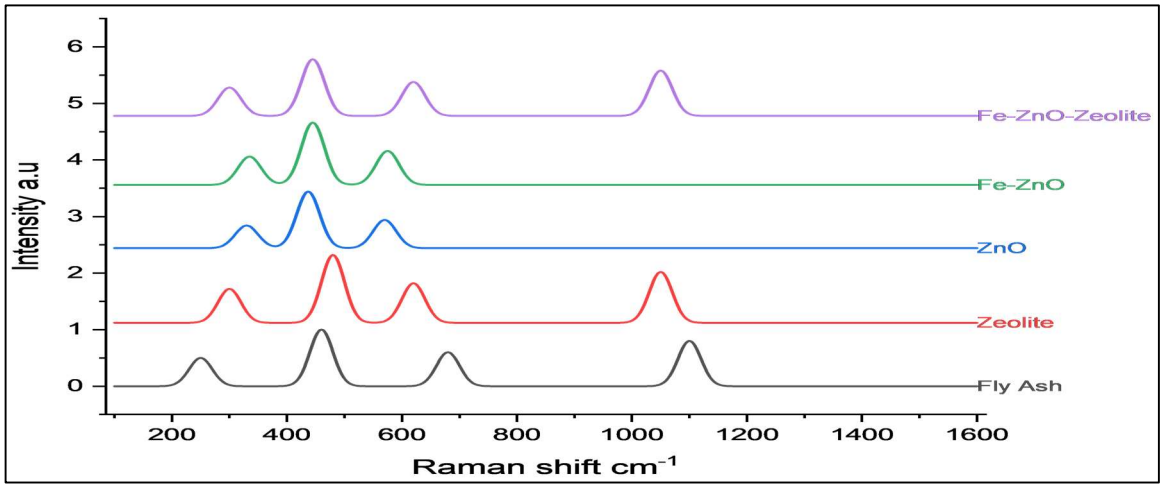

Fig. 5: XRD analysis of raw and synthesized materials.

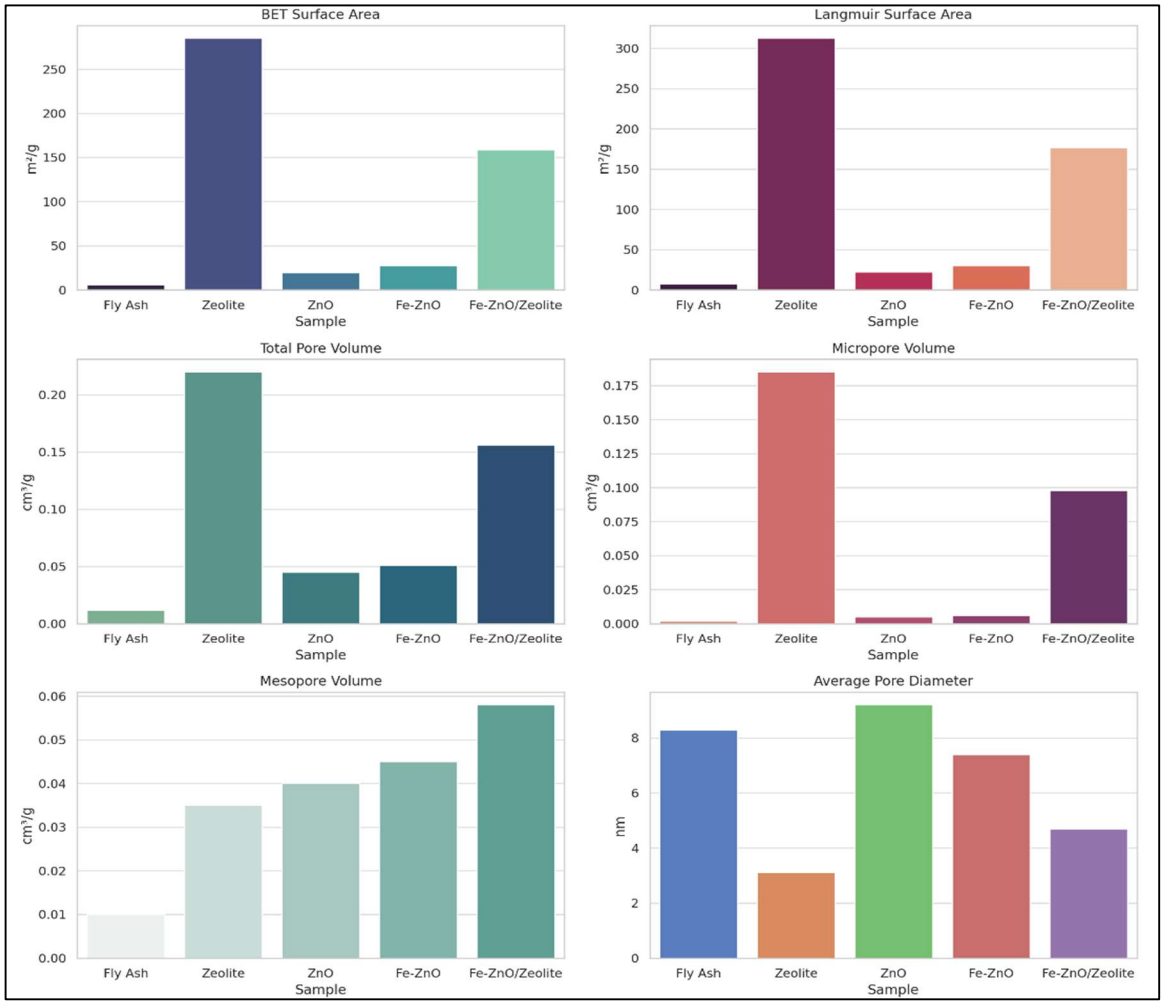

Fig. 6: BET (Brunauer–Emmett–Teller) surface area analysis of all samples.

BET Analysis

According to the nitrogen adsorption-desorption studies, fly ash, zeolite, ZnO, Fe-ZnO, and Fe-ZnO/zeolite have notably different surface properties. Fly ash has the lowest BET surface area (5.8 m^2/g) and total pore volume (0.012 cm^3/g), which predicts its amorphous and dense structure. The comparatively large average pore diameter (~8.3 nm) indicates a non-uniform mesoporous structure composed of randomly shaped, non-crystalline particles. Previous studies found that fly ash materials utilized as precursors in geopolymer synthesis have surface areas ranging from 3 to 10 m^2/g [59]. The synthesized zeolite in the current study has a high BET surface area (285.3 m^2/g), dominating micropore volume (0.185 cm^3/g), and a tiny average pore diameter (3.1 nm), indicating a microporous crystalline aluminosilicate framework. ZnO has a moderate surface area (19.5 m^2/g), a significant mesopore volume (0.040 cm^3/g), and a greater pore size (~9.2 nm). The surface areas of nanorods, nanoparticles, and other particles can range from 10 to 30 m^2/g, according to the literature [60]. The Fe-ZnO combination exhibits a slightly greater surface area (27.4 m^2/g) and enhanced mesopores (0.045 cm^3/g) as compared to pure ZnO, which has a somewhat smaller average pore diameter (~7.4 nm). Iron doping altered the surface shape and reduced the particle aggregation, thereby increasing the surface area. Previous studies found that Fe-doped ZnO nanoparticles have surface areas of up to ~30 m^2/g, depending on doping concentration [61]. The Fe-ZnO/zeolite composites have an intermediate BET surface area (158.7 m^2/g), which is greater than ZnO and Fe-ZnO but lower than zeolite. The material exhibits a balanced micro-porosity (0.098 cm^3/g) and meso-porosity (0.058 cm^3/g), with an average pore diameter of approximately 4.7 nm. Previous studies have found that similar composite materials (e.g., ZnO/zeolite or TiO_2/zeolite) have surface areas ranging from 100 to 200 m^2/g, which validates the findings of the present study [52].

Discussion along with future aspects of the study

This study describes the step-by-step synthesis of a novel Fe-ZnO/Zeolite composite, beginning with the modification of industrial waste into a valuable substance. A fusion-assisted hydrothermal technique was used to transform fly ash, a plentiful byproduct of coal burning, into zeolite. This approach can support the ideas of the circular economy as the synthesized zeolite can serve as a perfect support matrix for advanced material composites due to its high levels of crystallinity, microporosity, and thermal stability. The sol–gel process, reported for formulating homogeneous, high-purity particles with regulated size and shape, was used to develop ZnO nanoparticles in the second phase. The synthesized ZnO exhibited the characteristic hexagonal wurtzite structure, distinguished by its high surface activity and broad band gap. Iron (Fe) was used to dope ZnO, to further enhance its surface and photocatalytic properties. This doping process changed the electrical properties and added more surface flaws, increasing the adsorption potential of the material (Fe-ZnO). A hybrid composite was subsequently fabricated by integrating the Fe-doped ZnO into the zeolite framework, and this combination utilized Fe-ZnO catalytic and semiconducting properties in addition to the zeolite's large surface area and ion-exchange capacity. A material with both microporous and mesoporous properties was produced by the interaction of two phases, making it highly adaptable for uses such as catalysis and pollution removal applications.

The well-known characterization methods were used to verify the composite's morphology and structural integrity. The coexistence of crystalline phases and the preservation of structural order were verified via XRD analysis. Key functional groups and the interaction between ZnO, Fe, and the zeolitic matrix were disclosed by FTIR spectra. SEM pictures revealed that the nanoparticles were uniformly distributed and shaped throughout the zeolite surface. Characteristic peaks in Raman spectroscopy demonstrated the presence and integration of Fe-ZnO into the zeolite. The balanced micro-mesoporous structure of the composite, characterized by an average pore diameter and intermediate surface area, was further confirmed by BET surface analysis, indicating improved adsorption and catalytic performance.

This composite has a promising potential for the future in industrial and environmental applications, particularly in fields such as photocatalysis, gas adsorption, and wastewater treatment. To further improve performance, future research may focus on optimizing synthesis factors, including pH levels, calcination temperature, and Fe doping concentration. To evaluate the material's practical potential, pilot-scale manufacture and testing in authentic environmental settings will be essential to tailor the composite for specific targeted applications. Functional modifications through additional dopants or surface treatments may also be explored.

Conclusion

Keeping in view the findings of this study, there is reasonable ground to conclude that the synthesis of zeolites from fly ash and incorporation of Fe-doped ZnO presents a strategy/approach for fabricating composite materials with tailored properties. This approach not only offers an innovative way of waste management but also meets the criteria of matrix support for ZnO particles. The doping of ZnO with Fe effectively enhances its applicational potential, depending on the synergetic properties of Fe and ZnO. This waste-to-value synthesis pathway offers a cost-effective and sustainable approach for producing multi-functional materials. This piece of work can motivate young scientists to upcycle industrial waste into multifunctional materials to unlock the real-world applications.

Acknowledgments

We are thankful to all contributors for their active discussions and perceptions that contributed to the completion of this research work. We also acknowledge the support of the Department of Chemistry, Government College University, Faisalabad, for providing the essential resources for this work.

References

1. A. Moezzi, A.M. McDonagh and M.B. Cortie, zinc oxide particles: synthesis, properties and applications*, Chem. Eng. J*., **185**, 1 (2012).
2. S. Raha and M. Ahmaruzzaman, ZnO nanostructured materials and their potential applications: progress, challenges and perspectives*, Nano. Adv.,* **4**, 1868 (2022).
3. A. Singh, S. Kumar, V. Panghal, S. Arya and S. Kumar, Utilization of unwanted terrestrial weeds for removal of dyes*, Rasayan J. Chem.*, **12**, 1956 (2019).
4. K. Behpour, S. Ghoreishi, A. Gandomi-Niasar, N. Soltani and M. Salavati-Niasari, The inhibition of mild steel corrosion in hydrochloric acid media by two schiff base compounds*, J. Mat. Sci.,* **44**, 2444 (2009).
5. Y. Kang, Thermodynamic description of the Hg–Te system*, J. Alloys Com.,* **505**, 483 (2010).
6. A. Rahmati, A. Balouch Sirgani, M. Molaei and M. Karimipour, Cu-doped ZnO nanoparticles synthesized by simple Co-precipitation route*, Euro. Phy. J. Plus*, **129**, 250 (2014).
7. L.B. Chandrasekar, R. Chandramohan, M. Karunakaran and R. Vijayalakshmi, Synthesis and characterization of copper oxide and zinc oxide nanomaterials*, Nat. Sci. Mater.*, **1**, 18 (2016).
8. S. Kumar, S. Mukherjee, R. Kr Singh, S. Chatterjee and A. Ghosh, Structural and optical properties of sol-gel derived nanocrystalline Fe-doped ZnO*, J. App. Phy.,* **110**, 10 (2011).
9. A. Mancuso, O. Sacco, S. Mottola, S. Pragliola, A. Moretta, V. Vaiano and I. De Marco, Synthesis of Fe-doped ZnO by supercritical antisolvent precipitation for the degradation of azo dyes under visible light*, Inorg. Chim. Acta.*, **549**, 121407 (2023).
10. R. Saleh and N.F. Djaja, Transition-metal-doped ZnO nanoparticles: synthesis, characterization and photocatalytic activity under UV light*, Spectrochim. Acta. Mol. Biomol. Spectro.,* **130**, 581 (2014).
11. M. Maya-Treviño, J. Guzmán-Mar, L. Hinojosa-Reyes, N. Ramos-Delgado, M.I. Maldonado and A. Hernández-Ramírez, Activity of the ZnO–Fe_2O_3 catalyst on the degradation of dicamba and 2,4-d herbicides using simulated solar light*, Cera. Int.*, **40**, 8701 (2014).
12. H-L. Xia and F.Q. Tang, Surface synthesis of zinc oxide nanoparticles on silica spheres: preparation and characterization*, J. Phy. Chem.,* **107**, 9175 (2003).
13. J. Chen, Z. Feng, P. Ying and C. Li, ZnO clusters encapsulated inside micropores of zeolites studied by UV Raman and laser-induced luminescence spectroscopies*, J. Phy. Chem.,* **108**, 12669 (2004).
14. P.K. Dutta and M. Severance, Photoelectron transfer in zeolite cages and its relevance to solar energy conversion*, J. Phy. Chem. Letter.,* **2**, 467 (2011).
15. S.S Bukhari, J. Behin, H. Kazemian and S. Rohani, Conversion of coal fly ash to zeolite utilizing, microwave and ultrasound energies: a review*, Fuel*, **140**, 250 (2015).
16. X. Querol Carceller, N. Moreno, A. Alastuey, R. Juan Mainar, J.M. Andrés Gimeno, Á. López-Soler, C. Ayora, A. Medinaceli and A. Valero, Synthesis of high ion exchange zeolites from coal fly ash*, Geol. Acta*., **5**, 0049 (2007).
17. C. Zhou, C. Yan, Q. Zhou, H. Wang. and W. Luo, Producing a synthetic zeolite from secondary coal fly ash*, Env. Tech.,* **37**, 22 (2016).
18. S.S. Bukhari, S. Rohani. and H. Kazemian, Effect of ultrasound energy on the zeolitization of chemical extracts from fused coal fly ash, *Ultra. Sonochem.,* **28**, 47 (2016).
19. G. Kianpour, M. Salavati-Niasari and H. Emadi, Sonochemical synthesis and characterization of $NiMoO_4$ nanorods, *Ultra. Sonochem.,* **20**, 1 (2013).

20. M. Amiri, A. Pardakhti, M. Ahmadi-Zeidabadi, A. Akbari and M. Salavati-Niasari, Magnetic nickel Ferrite nanoparticles: green synthesis by urtica and therapeutic effect of frequency magnetic field on creating cytotoxic response in neural cell lines*, Colloids Surf. B Biointerfaces,* **172**, 244 (2018).
21. F. Mohandes and M. Salavati-Niasari, Sonochemical synthesis of silver vanadium oxide micro/nanorods: solvent and surfactant effects, *Ultra. Sonochem.,* **20**, 354 (2013).
22. T. Hussain, S.A.S. Chatha, M. Arshad, A.I. Hussain and A. Ali, Geopolymerization of raw fly ash to sodium zeolites for sequestration of As (iii) in aqueous medium*, Ind. J. Sci. Tech.,* **12**, 37 (2019).
23. D. Dutta, Optimization of process parameters and its effect on particle size and morphology of ZnO nanoparticle synthesized by sol–gel method*, J. Sol-Gel Sci. Tech.,* **77**, 48 (2016).
24. S. Fabbiyola, L.J. Kennedy, T. Ratnaji, J.J. Vijaya, U. Aruldoss and M. Bououdina, Effect of Fe-doping on the structural, optical and magnetic properties of ZnO nanostructures synthesised by Co-precipitation method*, Cera. Int.,* **42**, 1588 (2016).
25. F.S. de Dios, E.R. Morales, M.d.C.A. Cortaza, G.P. Hernández, E.V.M. Mandujano, E.M.L. Alejandro and L.R. Blanco, Improvement of photocatalysis using ZnO/zeolite nanocomposites for contaminant removal in aqueous media*, Des. Wat. Treat.,* **312**, 79 (2023).
26. A. Gogoi and S. Bhattacharjee. Room-temperature ethanol sensing by PVA/ZnS/ZnO: Fe nanocomposite synthesized by chemical precipitation technique, *J. Phy. Conf. Series.,* **2919**, 12001 (2024).
27. O.H. Abd-Elkader, M. Nasrallah, L. Aleya and M. Nasrallah, Biosynthesis, optical and magnetic properties of Fe-doped ZnO/C nanoparticles*, Surfaces*. **6**, 410 (2023).
28. A.K Kalita and S. Karmakar, Synthesis and structural characteristics of Fe doped ZnO nanoparticles at different molarities and temperatures*, J. Nan. Tech.*, 645 (2019).
29. K. Ojha, K, N.C. Pradhan and A.N. Samanta, Zeolite from fly ash: synthesis and characterization*, Bull. Mat. Sci.*, **27**, 555 (2004).
30. B. Jha and D.N. Singh, Fly ash zeolites: innovations, applications, and directions. 191 (2016).
31. M. Sitarz, W. Mozgawa and M. Handke, Rings in the structure of silicate glasses*, J. Mol. Str.,* **511**, 281 (1999).
32. R. Gayathri, G. Raja,and P. Rajeswaran, A simple and one step low cost microwave induced low cost grapheme modified CeO_2 photo electrodes for high-efficiency dye-sensitized solar cells*, Inorg. Chem. Comm.,* **120**, 108132 (2020).
33. T. Wedajo, A. Mekonnen and T. Alemu, Preparation and application of zeolite-zinc oxide nano composite for nitrate removal from groundwater*, J. Envi. Health Sci. Eng.,* **21**, 277 (2023).
34. Y.T. Prabhu, K.V. Rao, V.S.S. Kumar and B.S. Kumari, Synthesis of ZnO nanoparticles by a novel surfactant assisted amine combustion method*, Adv. Nano.,* **2**, 45 (2013).
35. M.I. Khalil, M.M. Al-Qunaibit, A.M. Al-Zahem and J.P. Labis, Synthesis and characterization of ZnO nanoparticles by thermal decomposition of a curcumin zinc complex*, Ara, J. Chem.,* **7**, 1178 (2014).
36. S. Kanchana, M.J. Chithra, S. Ernest and K. Pushpanathan, Violet emission from Fe doped ZnO nanoparticles synthesized by precipitation method*, J. Lum.*, **176**, 6 (2016).
37. C. Wang, H. Shi and Y. Li, Synthesis and characteristics of natural zeolite Supported Fe^{3}_{+}-TiO^{2} photocatalysts*, App. Sur. Sci*., **257**, 6873 (2011).
38. X. Querol, N. Moreno, J, Umaña, A. Alastuey, E. Hernández, A. Lopez-Soler and F. Plana, Synthesis of zeolites from coal fly ash: an overview*, Int. J. C. Geo.,* **50**, 413 (2002).
39. T. Hussain, A.I. Hussain, S.A.S. Chatha, A. Ali, M. Rizwan, S. Ali, P. Ahamd, L. Wijaya and M.N. Alyemeni, Synthesis and characterization of Na-zeolites from textile waste ash and its application for removal of lead (Pb) from wastewater*, Int. J. Env. Res. Pub. Health*, **18**, 3373 (2021).
40. M. Gualtieri, PhD Dissertation, *Synthesis and Characterization of Zeolite Films and Membranes*, Lulea Tekniska University, (2006).
41. M.B. Varela, S.M. Ramírez, I. Ereña, M. Gener and P. Carmona, Characterization and pozzolanicity of zeolitic rocks from two cuban deposits*, App. Clay Sci*., **33**, 149 (2006).
42. Z.M. Khoshhesab, M. Sarfaraz and M.A. Asadabad, Preparation of ZnO nanostructures by chemical precipitation method*. Synth. React. Inorg. Met.-Org. Chem*., **41**, 814 (2011).
43. N. Hongsith, E. Wongrat, T. Kerdcharoen and S. Choopun, Sensor response formula for sensor based on ZnO nanostructures*, Sen. Act. Chem.,* **144**, 67 (2010).
44. H. Xu, D. Zhang and F. Wu, Photocatalytic activity of nano-ZnO loaded with Ag and Fe immobilized on ZSM-5*. Des, Wat. Treat.,* **74**, 308 (2017).
45. O.M. Linder-Patton, T.J. de Prinse, S. Furukawa, S.G. Bell, K. Sumida, C.J. Doonan and C.J.

Sumby, Influence of nanoscale structuralisation on the catalytic performance of ZiF-8: a cautionary surface catalysis study, *CrystEngComm*., **20**, 4926 (2018).
46. N.M. Musyoka, Zeolite A, X and cancrinite from South African coal fly ash: mechanism of crystallization, routes to rapid synthesis and new morphology, (2012).
47. K. Sangita, B. Prasad and G. Udayabhanu, Synthesis of zeolite from waste fly ash by using different methods, *Asi. J. Chem.,* **28**, 1435 (2016).
48. Y. Costa-Marrero, M.B. De Andrade, J. Ellena, J. Duque-Rodríguez, T. Farías and G. Autié-Castro, Zeolite/ZnO composites based on a cuban natural clinoptilolite and preliminary evaluation in methylene blue adsorption, *Mat. Res. Ex*., **7**, 015066 (2020).
49. E. Alizadeh and H. Baseri, Photocatalytic degradation of sumatriptan succinate by ZnO, Fe-doped ZnO and TiO_2-ZnO nanocatalysts, *Mat. Chem. Hor.*, **1**, 7 (2022).
50. M. Pratiwi, N. Afifah and R. Saleh, Enhanced stability and photocatalytic performance of transition metal-doped ZnO with magnetite nanoparticle and zeolite, *Mat. Sci. Eng., IOP Publishing* (2017).
51. R. Al-Gaashani, H. Alyasi, F. Karamshahi, S. Simson, Y. Tongb, V. Kochkodan and J. Lawler, Nickel removal from synthetic wastewater by novel zeolite-doped magnesium-iron-and zinc-oxide nanocomposites by hydrothermal-calcination technique, *Sci. Rep.,* **14**, 30954 (2024).
52. M. Pratiwi, N. Afifah and R. Saleh, Decoloration of organic dyes using zeolites supported Fe-doped ZnO under UV light irradiation, *AIP Conference Proceeding, AIP Publishing* (2017).
53. S. Mustapha, M. Ndamitso, A. Abdulkareem, J. Tijani, D. Shuaib, A. Mohammed and A. Sumaila, Comparative study of crystallite size using williamson-hall and debye-scherrer plots for ZnO nanoparticles, *Adv. Nat. Sci. Nanotech.,* **10**, 45013 (2019).
54. R. Monsef and M. Salavati-Niasari, Tuning architectural synergy reactivity of nano-tin oxide on high storage reversible capacity retention of ammonium vanadate nanobelt array cathode for lithium-ion battery, *Mat. Sci Eng.,* **310**, 117743 (2024).
55. M. Ritz, Infrared and Raman spectroscopy of Mullite ceramics synthesized from fly ash and kaolin, *Minerals*, **13**, 864 (2023).
56. S. Sadiq, S.A.S. Chatha, S. Ali, M. Shahid and P.K. Sarker, Microwave assisted synthesis of fly ash based zeolites for degradation of reactive blue 19 dye from wastewater, *Sci. Rep.*, **15**, 16028 (2025).
57. T. Tran, X.H. Vu, T.L. Ngo, T.T.H. Pham, D.D. Nguyen and V.D. Nguyen, Enhanced Raman scattering based on a ZnO/Ag nanostructured substrate: an in-depth study of the sers mechanism, *Phy. Chem. Chem. Phy.,* **25**, 15941 (2023).
58. F. Lekoui, S. Hassani, E. Garoudja, R. Amrani, W. Filali, O. Sifi and S. Oussalah, Elaboration and characterization of pure ZnO, Ag: ZnO and Ag-Fe: ZnO thin films: effect of Ag and Ag-Fe doping on ZnO physical properties, *Rev. Mex. Fís.,* **69**, 5 (2023).
59. S. Wang and H. Wu, Environmental-Benign utilisation of fly ash as low-cost adsorbents, *J. Haz. Mat.,* **136**, 482 (2006).
60. A. Kołodziejczak-Radzimska and T. Jesionowski, Zinc oxide-from synthesis to application: a review, *Materials,* **7**, 2833 (2014).
61. N. Madkhali, Analysis of structural, optical, and magnetic properties of (Fe, Co) Co-doped ZnO nanoparticles synthesized under UV light, *Con. Mat.*, **7**, 63 (2022).